

Learning Multi-Modal Image Registration without Real Data

Malte Hoffmann¹, Benjamin Billot², Juan Eugenio Iglesias^{1,2,3}, Bruce Fischl^{1,3}, and
Adrian V. Dalca^{1,3}

¹ A. A. Martinos Center for Biomedical Imaging, Massachusetts General Hospital, Harvard
Medical School, USA

² Centre for Medical Image Computing, University College London, United Kingdom

³ Computer Science and Artificial Intelligence Laboratory, Massachusetts Institute of Technology,
USA

Abstract. We introduce a learning-based strategy for multi-modal registration of images acquired with any modality, without requiring real data during training. While classical registration methods can accurately align multi-modal image pairs, they solve a costly optimization problem for every new pair of images. Learning-based techniques are fast at test time, but can only register images of the specific anatomy and modalities they were trained on. In contrast, our approach leverages a generative model to synthesize label maps and gray-scale images that expose a network to a wide range of anatomy and contrast during training. We demonstrate that this strategy enables robust registration of arbitrary modalities, without the need to retrain for a new modality. Critically, we show that input labels need not be of actual anatomy: training on randomly synthesized shapes, or *supervoxels*, results in competitive registration performance and makes the network agnostic to anatomy and contrast, all while eradicating the need for real data. We present extensive experiments demonstrating that this strategy enables registration of modalities not seen during training and surpasses the state of art in cross-contrast registration. Our code is integrated with the *VoxelMorph* library at <http://voxelmorph.csail.mit.edu>.

Keywords: deformable image registration · modality independence · training without data · avoiding retraining

1 Introduction

Image registration estimates spatial correspondence between pairs of images and is a fundamental component of many medical image analysis pipelines involving data acquired across modalities, subjects, or time. For example, neuroimaging segmentation packages [14,16] often perform deformable registration to a probabilistic atlas, before neuroanatomical structures are labeled. In this work, we focus on the challenging task of multi-modal deformable (nonlinear) registration.

Classical approaches typically solve an iterative optimization problem to estimate a deformation from a moving image to a fixed image (or atlas). The optimization function generally combines an image similarity metric, which compares the warped moving and fixed images, and a regularization term that encourages well-behaved deformations [3,5,26,35,37,40]. The exact choice of these terms and optimization strategy depends on the particular task. Simple image similarity metrics such as mean squared difference (MSD) or normalized cross-correlation (CC) [5] perform well on image pairs with similar contrast, for example if both

moving and fixed images are T1-weighted magnetic resonance imaging (MRI) scans [22]. For images acquired with different modalities, metrics such as mutual information (MI) [41] or correlation ratio [33] have been developed, but are less accurate for multi-modal deformable registration than their unimodal counterparts for unimodal registration. Unfortunately, classical registration methods require significant runtime, since they solve the optimization problem for every pair of images independently.

Recent learning-based techniques, mostly using convolutional neural networks (CNNs), address this runtime drawback by learning a function that directly outputs the deformation field given an image pair [6,12,24,34,38,42]. After training, evaluating this function is efficient, enabling fast registration. *Supervised* models learn to reproduce simulated warps or deformation fields estimated by classical methods [24,34,38]. In contrast, *unsupervised* models minimize loss functions similar to those used by classical methods [6,12,23,42] such as normalized mutual information (NMI) [17] that can drive inter-modal registration. In another multi-modal registration paradigm, networks have been used to synthesize one modality from the other, so that within-modality loss functions can then be used for the subsequent nonlinear registration [20,31]. Unfortunately, these learning-based approaches depend on the data seen during training and do not perform well on unobserved modalities. For example, a model trained on pairs of T1- and T2-weighted MRI scans will not perform well at T1 to a computer-tomography (CT) registration and would require re-training with MR and CT data.

Data augmentation strategies expose a model to a wider range of variability than the training data encompasses, for example by randomly altering voxel intensities or applying affine and non-linear deformations [8,10,36,44,45]. However, these methods still require specific input modalities. Similarly, transfer learning has been used to extend a trained network to new modalities, but do not remove the need for data acquired with the specific target modality [21].

In this work, we propose **VoxelMorph-Synth**: a modality-agnostic learning framework for registering image pairs both within and across a range of contrasts, *without* the need to retrain given a new modality. We introduce a generative model that first synthesizes random label maps that resemble variable-shaped supervoxels. Then, conditioned on these labels, our model generates images of arbitrary contrasts, deformations, and artifacts. A neural network then learns to match corresponding shapes regardless of image-contrast or anatomical characteristics, making it applicable to a wide range of real image contrasts. We compare this model to classical and learning-based baselines and demonstrate state-of-the-art performance and runtime in multi-modal brain MRI registration. The proposed framework improves on classical multi-modal loss functions, despite the fact that the network has never been exposed to the exact contrast or anatomy in the images being registered. Our code is available as part of the **VoxelMorph** library at <http://voxelmorph.csail.mit.edu>.

2 Method

2.1 General Learning-based Registration Framework

Let m and f be a moving and fixed (or reference) 3D image, respectively. In this work, we build on learning-based registration frameworks and focus on deformable (non-linear) registration. Specifically, we use a neural network $h_{\theta}(m, f) = \phi_{\theta}$, with parameters θ , that outputs the deformation ϕ_{θ} for image pair $\{m, f\}$. In training, the network is given a new pair of images $\{m, f\}$ at each iteration, and network parameters are updated with stochastic

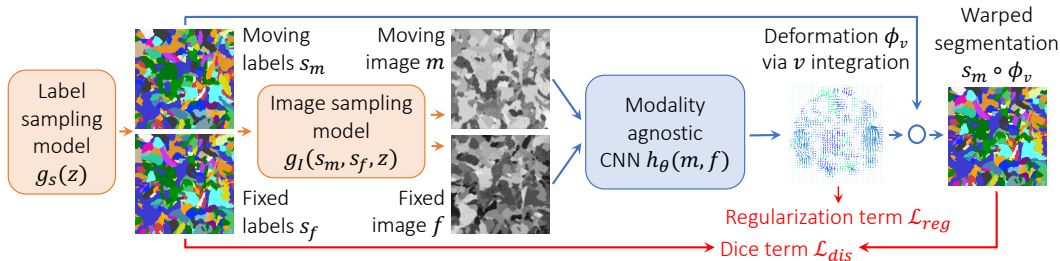


Fig. 1. Proposed unsupervised learning framework for modality-agnostic registration. We synthesize a pair of label maps $\{s_m, s_f\}$ and corresponding images $\{m, f\}$ based on a generative model that covers a wide range of shapes and contrasts. These are used to train a U-Net-style network for diffeomorphic registration adapted from the *VoxelMorph* architecture.

gradient descent, based on a loss function $\mathcal{L}(\theta; m, f)$ similar to classical cost functions. Typically, these contain an image dissimilarity term $\mathcal{L}_{dis}(m \circ \phi_\theta, f)$ which penalizes the difference between the warped image and the fixed in terms of appearance, and a regularization term $\mathcal{L}_{reg}(\phi)$ that encourages smooth deformation fields:

$$\mathcal{L}(\theta; m, f) = \mathcal{L}_{dis}(m \circ \phi_\theta, f) + \lambda \mathcal{L}_{reg}(\phi_\theta), \quad (1)$$

where $\phi_\theta = h_\theta(m, f)$ is the network output, and λ controls the weighting of these terms. Unfortunately, networks only learn to output reasonable deformations for contrasts and anatomy they observe during training. We address this dependency using the following generative model.

2.2 Modality-Agnostic Strategy

We achieve modality-agnostic registration by requiring *no* real training data, but instead synthesizing arbitrary contrasts and shapes through a generative process. The framework is summarized in Figure 1. We first synthesize two paired label (segmentation) maps $\{s_m, s_f\}$ using a function $g_s(z) = \{s_m, s_f\}$ given random seed z . We define the function $g_i(s_m, s_f, z) = \{m, f\}$ to synthesize two intensity volumes based on the given segmentation maps $\{s_m, s_f\}$ and seed z .

This generative process resolves the limitations of existing methods as follows. First, we train a registration network $h_\theta(m, f)$ using the generated data. This exposes the model to arbitrary synthesized contrasts and shapes at each iteration, making it robust to a variety of contrasts and anatomy. Second, the label maps $\{s_m, s_f\}$ enable a (soft) Dice-based [25] similarity loss that measures label overlap:

$$\mathcal{L}'_{dis}(\phi, s_m, s_f) = -\frac{2}{J} \sum_{j=1}^J \frac{|(s_m^j \circ \phi) \odot s_f^j|}{|(s_m^j \circ \phi) \oplus s_f^j|}, \quad (2)$$

where s^j represents the one-hot encoded label j of segmentation map s , and \odot and \oplus denote the voxel-wise multiplication and addition, respectively.

We complete the model by parameterizing the deformation ϕ with a stationary velocity field (SVF) v , which is integrated within the network to obtain a diffeomorphic (and thus invertible) deformation [2,3,12]. We regularize the field ϕ using $\mathcal{L}_{reg}(\phi) = \frac{1}{2} \|\nabla \mathbf{u}\|^2$, where \mathbf{u} is the displacement of deformation field $\phi = Id + \mathbf{u}$.

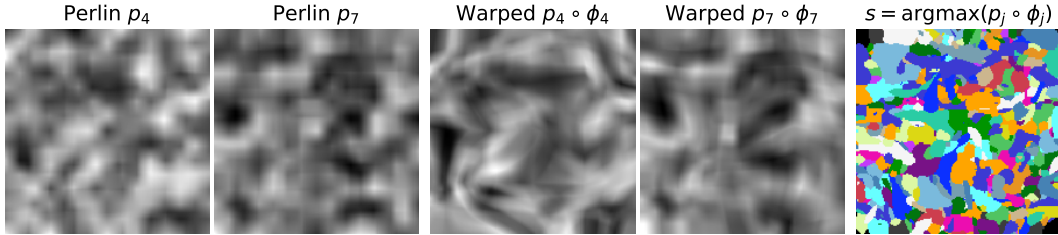


Fig. 2. Generation of random *supervoxel* segmentations. A set of J smoothly varying 3D Perlin-noise images p_j ($j = 1, 2, \dots, J$) is sampled (here showing two example images), then warped by random deformation fields ϕ_j to cover a range of spatial scales and shapes. The final label map s is obtained by voxel-wise assignment of the label j with the highest intensity across the warped images $p_j \circ \phi_j$.

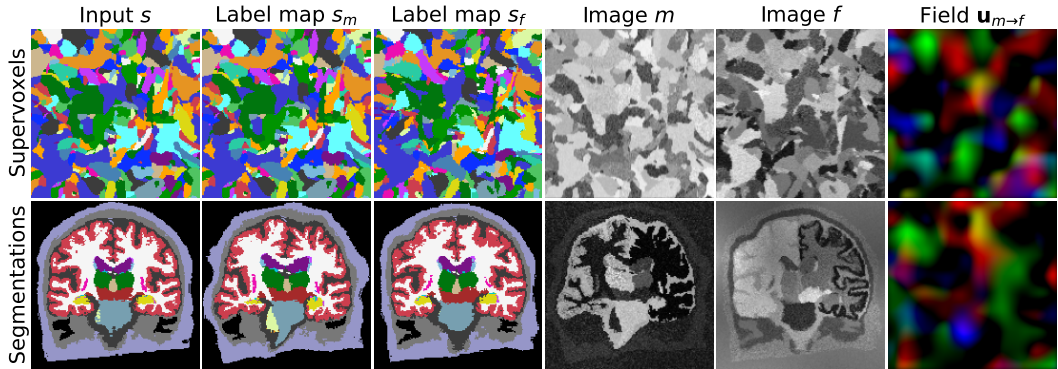


Fig. 3. Example of synthetic training data (2D slices taken from volumes). Top row: *supervoxel* segmentations and images. Bottom: if available, the generative process can be initialized by existing label maps. Two label maps $\{s_m, s_f\}$ and corresponding images $\{m, f\}$ with arbitrary contrast are generated from s ; random shapes or a segmentation. The model takes $\{s_m, s_f\}$ as input and is trained to predict the displacement field $\mathbf{u}_{m \rightarrow f}$ (red: left-right, green: inferior-superior, blue: posterior-anterior).

2.3 Model Details

Label Maps. We generate J smoothly varying Perlin-noise [28] images p of the same size using $g_s(z)$ given a random seed z . Each image p is warped by a random smooth deformation field ϕ_p (described below), to approximately span the appropriate range of spatial scales and shapes found in anatomical images. As shown in Figure 2, we obtain a segmentation map s by assigning the label with the highest intensity among the noise images p for each voxel, i.e. $s = \arg \max_j (p_j \circ \phi_{p_j})$.

Alternatively, anatomical label maps for the anatomy of interest, for example from a public dataset, can be used if available. In this case, $g_s(\cdot, z)$ simply selects a segmentation at random based on seed z (Figure 3). We emphasize that no real images are involved in this process.

Given a selected label map s , we generate two new label maps. First, we deform s with a random smooth diffeomorphic transformation ϕ_m using nearest-neighbor interpolation to

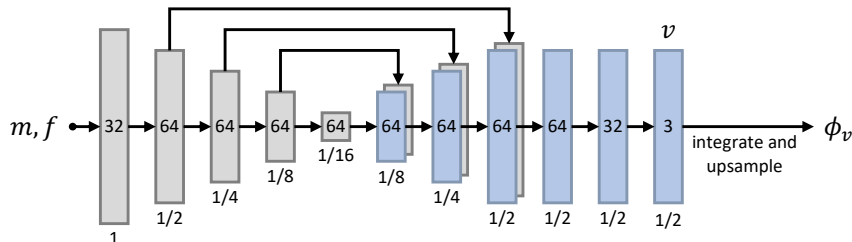


Fig. 4. Convolutional U-Net architecture implementing $g_\theta(m, f)$. Each block represents a volume created using a 3D convolution with n filters (written on each box) and a LeakyReLU layer with parameter 0.2. The encoding convolutions (stride 2) reduce the resolution to $1/16$ relative to the inputs m, f . In the decoder, each convolution (stride 1) is followed by an upsampling layer, bringing the resolution back to $1/2$. Arrows represent skip connections which concatenate encoder and decoder layers. The deformation field ϕ_v is obtained by integrating and upsampling v . All convolutions use $3 \times 3 \times 3$ kernels.

produce the warped segmentation map $s_m = s \circ \phi_m$. An analogous process is then used to produce s_f .

Synthetic Images. For each pair of label maps $\{s_m, s_f\}$, we synthesize gray-scale images $\{m, f\}$ inspired by generative models of MR imaging [4,8,39] as follows. Given a segmentation map s , we draw the intensities of all voxels associated with each label j as independent samples from the normal distribution $\mathcal{N}(\mu_j, \sigma_j^2)$. The mean μ_j and variance σ_j^2 for each label are uniformly sampled from continuous distributions $\mathcal{U}(a_\mu, b_\mu)$ and $\mathcal{U}(a_\sigma, b_\sigma)$, respectively, where a_μ, b_μ, a_σ , and b_σ are hyperparameters. To simulate partial volume effects, the image is blurred by convolving it with an anisotropic Gaussian kernel $K(w_{i=1,2,3})$ whose full widths at half maximum w_i are sampled such that $w_i = \mu_w + |\tilde{w}|$ with $\tilde{w} \sim \mathcal{N}(0, \sigma_w^2)$.

For MRI applications, each image is optionally corrupted by voxel-wise multiplication with a spatially varying intensity-bias field B [7,19]. To form B , each voxel is independently sampled from a normal distribution $\mathcal{N}(0, \sigma_B^2)$ at reduced size $d_1^B \times d_2^B \times d_3^B$ where $\sigma_B \sim \mathcal{U}(0, b_B)$ is sampled uniformly. This low resolution field is upsampled trilinearly to match the image size, and the exponential of each voxel is taken to yield non-negative values. We obtain the final images m and f through min-max normalization and gamma augmentation using the normally distributed parameter $\gamma \sim \mathcal{N}(0, \sigma_\gamma^2)$ such that $m = \tilde{m}^{\exp(\gamma)}$, where \tilde{m} is the normalized moving image, and similarly for the fixed image (Figure 3).

Random Transforms. Transforms ϕ_p, ϕ_m and ϕ_f are obtained by integrating random SVFs v_p, v_m and v_f using a GPU implementation of scaling and squaring with 5 steps [12]. We draw the voxel values of the SVFs as independent samples of a normal distribution $\mathcal{N}(0, \sigma_v^2)$ at reduced size $d_1^v \times d_2^v \times d_3^v \times 3$, where $\sigma_v \sim \mathcal{U}(0, b_v)$ is sampled uniformly. We interpolate each transform linearly to full resolution and blur it isotropically, using parameters μ_ϕ, σ_ϕ (similarly to μ_w, σ_w).

Hyperparameters. The generative process encompasses a number of parameters. During training, we sample these based on the hyperparameters presented in Table 1. These values were not chosen to simulate realistic anatomy or a particular physically-achievable image contrast. In contrast, we selected hyperparameters visually to yield shapes and contrasts that far exceed a realistic image range, to increase the robustness of the network [10].

Table 1. Hyperparameter values used in our experiments. Spatial measures are in voxels. We use a volume size of $160 \times 160 \times 192$ and sample v and B at relative resolutions $1/16$ and $1/40$, respectively.

Hyperparameter	a_μ	b_μ	a_σ	b_σ	b_B	μ_w	σ_w	σ_γ	b_v	μ_ϕ	σ_ϕ
Value	25	225	5	25	0.3	0.1	2	0.25	6	1	3

Implementation. A neural network for diffeomorphic registration was adapted from the `VoxelMorph` framework available online [6,12]. Briefly, a 3D U-Net architecture [36] takes two images as input and predicts an SVF v which is integrated at half resolution to obtain a prediction of the diffeomorphic displacement field ϕ_v . We implemented the model shown in Figure 4 to run on a GPU using Keras [11] with a TensorFlow backend [1].

3 Experiments

We evaluate several variants of our learning framework for deformable registration and compare it to a set of baselines in a variety of datasets. These datasets were chosen to include several different modalities and levels of processing to assess the robustness of the methods across a range of scenarios.

3.1 Experimental Setup

Data. We compile 3T-MRI datasets from the Human Connectome Aging Project (HCP-A) [9,18] and the Alzheimers Disease Neuroimaging Initiative (ADNI) database [43]. HCP-A includes T1-weighted MPRAGE [27] and T2-weighted T2SPACE 3D brain scans from the same subjects; no preprocessing is applied, except downsampling from 0.8 to 1 mm isotropic resolution. ADNI includes T1-weighted, gradient-unwarped and bias-field corrected MPRAGE scans at $\sim(1 \text{ mm})^3$ resolution that we resample to 1 mm isotropic. We also use in-house proton-density (PD) scans from 8 subjects, skullstripped and with manual labelings. Finally, we derive 40 label maps for synthesizing brains based on distinct-subject MPRAGE scans from the Buckner40 dataset [15] using SAMSEG [29]. As we focus on deformable registration, all images are mapped into a common affine space [14,32].

Setup. We run experiments on combinations of these datasets: T1-to-T2 and T1-to-PD, with full head or skull-stripping to assess robustness to extracerebral structures. For validation and analysis, we randomly select images from 10 (8 for PD) subjects, leading to 90 (56) cross-subject registration pairs for each combination. All presented results are evaluated on an additional, held-out dataset of the same size for T1-to-T2, and all PD scans.

Baselines. We first test classical methods using ANTs’s `SyN` [5] with default parameters and MI as similarity metric [30]. We also employ `NiftyReg` [26] with default cost function (NMI) and parameters and enable its diffeomorphic model with SVF integration, as in our approach.

We train a learning-based method based on `VoxelMorph`, using the same architecture as `VoxelMorph-Synth` but with NMI as a classical loss and real data (`vm-nmi`): 100 skullstripped T1-T2 image pairs from HCP-A that did not overlap with the validation sets.

VoxelMorph-Synth Variants. For data- and shape-agnostic training, we generate $\{s_m, s_f\}$ from one of 100 *supervoxel* segmentations s at each iteration (`sm-svx`). Each s is synthesized

from 27 Perlin-noise images p , resulting in 27 separate labels which we all include in the loss \mathcal{L}_{dis} . Since brain segmentations are often available (even if not for the target modality), we also test our framework when starting with a set of brain-anatomy label maps instead of supervoxels. We investigate two variants for generating $\{s_m, s_f\}$ before random warping: starting from a pair of label maps from different subjects $\{s_1, s_2\}$ (**sm-brain-ds**), or starting with the same single segmentation for both maps (**sm-brain-ss**). Half of the label maps include brain anatomy only, and the other half also include extra-cerebral labels. For **sm-brain** models, we include the largest cerebral labels in \mathcal{L}_{dis} (see below). No acquired data is used.

Assessment. We measure registration accuracy using the Dice metric D [13] across a representative subset of brain structures: amygdala, brainstem, caudate, ventral DC, cerebellar white matter and cortex, pallidum, cerebral white matter and cortex, hippocampus, lateral ventricle, putamen, thalamus, cerebrospinal fluid, 3rd and 4th ventricle, and choroid-plexus. For **sm-brain** models, the latter three small structures are excluded from the training loss \mathcal{L}_{dis} . Scores of bilateral structures are averaged. We also compute the proportion of locations where the deformation ϕ is folded, i.e. those with a Jacobian J_ϕ such that $\det(J_\phi) \leq 0$.

Framework Analysis. Using a validation set, we analyze two model properties. First, we train with various regularization weights $\lambda \in [0, 10]$ and evaluate accuracy across: (1) all above-listed labels, (2) only the largest 14 structures optimized in \mathcal{L}_{dis} . Second, we vary the deformation range by training variants of our model with halved and doubled maximum SD relative to the default value b_v , respectively.

3.2 Results

Figure 5 shows mean Dice scores across structures for the competing methods on the three inter-modality problems. The proposed model is comparable or superior to **ANTs** and **NiftyReg** across datasets, despite never having been exposed to real MR images or anatomical shapes. Even better results are obtained by **sm-brain-ss**, which exploits the anatomical information in a set of brain labels, to provide a boost of 6 Dice points over **ANTs** (T1-T2, 5 with skullstripping) and 3 over **NiftyReg** (T1-T2, 5 with skullstripping). In a paired t-test, this improvement is significant across datasets ($p < 10^{-15}$ in all cases, except $p < 10^{-6}$ for T1-PD).

The learning-based method **vm-nmi** using mutual information provides accuracy comparable to that of **ANTs** and **NiftyReg** on skull-stripped data, but its accuracy drops considerably on unprocessed whole-brain scans. As expected, this approach completely fails when tested on a pair of contrasts (T1-to-PD) different from what was used in training (T1-to-T2). Typical T1-to-T2 registration results are shown in Figure 6.

We also analyze a model that was trained in a supervised fashion. As with other variants, images m, f are generated by deforming the same label map, but we use MSD between the true and predicted deformation fields as a loss. We do not report these results because this model considerably under-performs compared to other **sm** variants. This is likely because in many areas of the image, such as the background or middle of the white matter, there is no signal to drive the network to the ground truth deformation.

In our experiments, all learning-based models require less than a second per registration on an Nvidia Tesla V100 GPU, while the classical methods typically take ~ 0.5 hours on a 3.3-GHz Intel Xeon CPU (single-threaded).

In summary, **VoxelMorph-Synth** achieves registration accuracy comparable or superior to classical methods but is orders of magnitude faster. While learning-based methods like

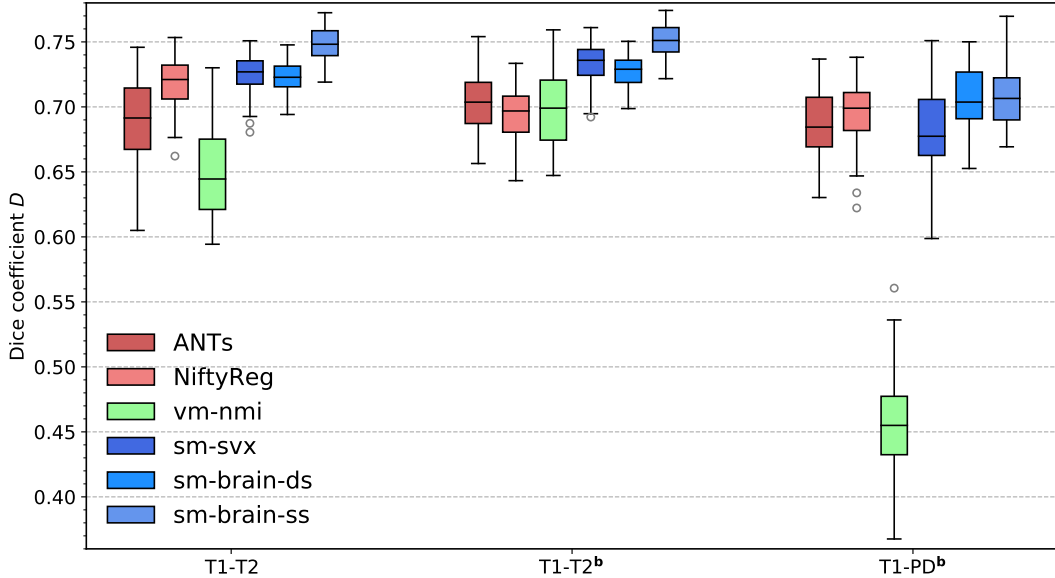


Fig. 5. Multi-modal registration accuracy. We evaluate the average Dice overlap for 90 T1-T2 test-image pairs from HCP-A. For T1-PD registration, we combine 8 in-house PD scans with randomly chosen ADNI T1 subjects to yield 56 registration pairs. The letter **b** indicates skullstripped datasets.

VoxelMorph can only register modalities observed during training, the proposed approach registers unseen modalities with optimal performance.

3.3 Analyses

Figure 7 compares registration performance for various training settings. The model trained on a mixture of whole-brain and skull-stripped images performs as well as those trained specifically for each scenario (Figure 7.a). The method is not particularly sensitive to the strength of the simulated deformation fields (Figure 7.b). Figure 7.c shows that with reducing regularization, accuracy increases for the large structures used in \mathcal{L}_{dis} . When we include smaller structures, the mean overlap D reduces for $\lambda < 1$, as the network then focuses on optimizing the training structures. This does not apply to **sm-svx**, which is agnostic to anatomy and trained on all labels present in the *supervoxel* segmentations.

Finally, we find a small proportion of folding voxels, decreasing with increasing λ (Figure 8). For all results presented, we choose an optimal value of $\lambda = 1$, where the proportion of folding voxels is $\sim 10^{-6}$ at our numerical precision.

4 Conclusion

We propose an unsupervised learning framework for modality-agnostic registration. Training a registration network on samples of a generative model of generic contrast and shape, we achieve multi-modal registration accuracy that matches or exceeds the state-of-the-art in classical and learning-based methods. This performance is achieved although our network never had access to the contrasts present in the test set. Therefore, the framework does not

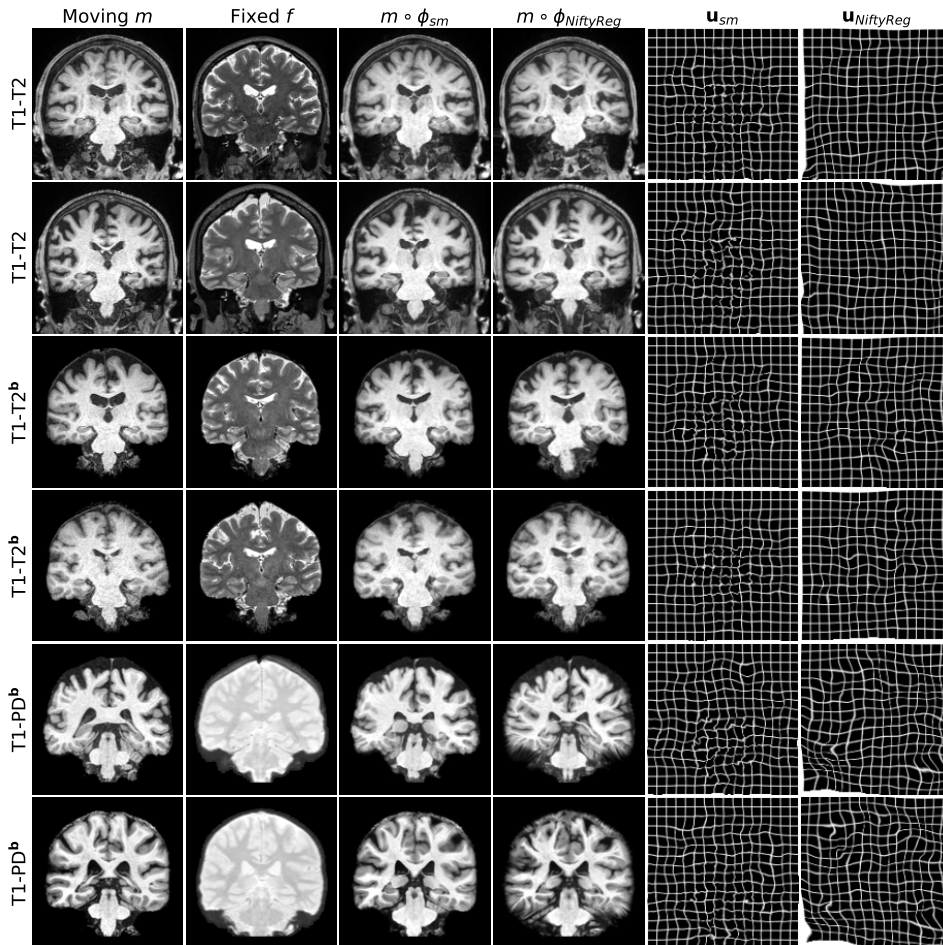


Fig. 6. Typical multi-modal registration results for *sm-brain-ss* (*sm*) and *NiftyReg*. Each row shows a different registration pair from the source datasets indicated on the left, which were skull-stripped when marked with the letter **b**.

require re-training for a new modality, which represents an improvement over current deep learning methods.

While the proposed method addresses significant drawbacks of classical and learning-based methods for multi-modal registration, it can be improved in several ways. Since some data is often available at training, we will investigate whether combining real images and synthetic *supervoxel* data improves registration accuracy. We will consider combinations of our training loss with classical registration metrics, such as NCC for intra-modal, or NMI for inter-modal registration. Finally, we will quantify the effects of the geometric properties of the supervoxels on warp accuracy and robustness in brain images, images of other body parts, and non-medical images. We anticipate that the combination of these advances will enable a single registration algorithm capable of accurately aligning unprocessed input images of any modality and body part.

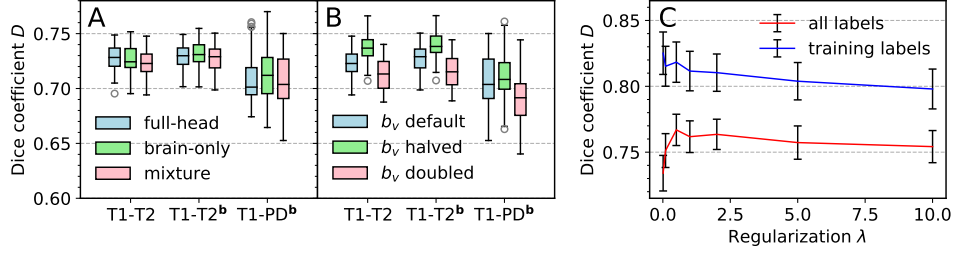


Fig. 7. Framework analysis based on overlap of anatomical structures for various training settings: **A** Different sets of anatomical segmentations s . **B** Halved and doubled ranges b_v of synthesized deformations relative to the default value. **C** Regularization parameters λ .

Acknowledgements

This research was supported by the European Research Council (ERC Starting Grant 677697, project BUNGEE-TOOLS), and by the National Institutes of Health (NIH) grant U01-AG052564.

Further Support was provided in part by the BRAIN Initiative Cell Census Network grant U01-MH117023, the National Institute for Biomedical Imaging and Bioengineering (P41-EB015896, 1R01-EB023281, R01-EB006758, R21-EB018907, R01-EB019956), the National Institute on Aging (1R56-AG064027, 1R01-AG064027, 5R01-AG008122, R01-AG016495), the National Institute of Mental Health the National Institute of Diabetes and Digestive and Kidney Diseases (1-R21-DK-108277-01), the National Institute for Neurological Disorders and Stroke (R01-NS0525851, R21-NS072652, R01-NS070963, R01-NS083534, 5U01-NS086625, 5U24-NS10059103, R01-NS105820), and was made possible by the resources provided by Shared Instrumentation Grants 1S10-RR023401, 1S10-RR019307, and 1S10-RR023043. Additional support was provided by the NIH Blueprint for Neuroscience Research (5U01-MH093765), part of the multi-institutional Human Connectome Project. In addition, BF has a financial interest in CorticoMetrics, a company whose medical pursuits focus on brain imaging and measurement technologies. BF’s interests were reviewed and are managed by Massachusetts General Hospital and Partners HealthCare in accordance with their conflict of interest policies.

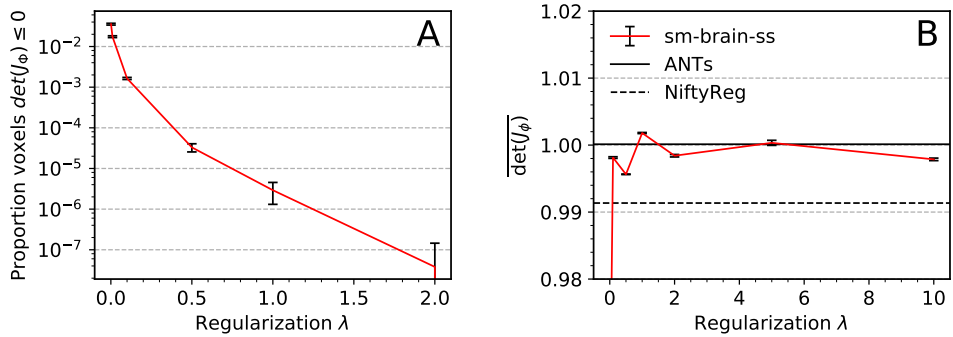


Fig. 8. Regularization analysis. **A** Proportion of locations where the deformation field ϕ is folded, i.e. voxels with a Jacobian J_ϕ such that $\det(J_\phi) \leq 0$ (of 4.9×10^6 voxels). **B** Average Jacobian determinant. For $\lambda \geq 1$, the deviation from the the ideal value $\det(J_\phi) = 1$ is below 2×10^{-3} .

References

1. Abadi, M., Barham, P., Chen, J., Chen, Z., Davis, A., Dean, J., et al.: Tensorflow: A system for large-scale machine learning. In: 12th {USENIX} Symposium on Operating Systems Design and Implementation ({OSDI} 16). pp. 265–283 (2016)
2. Arsigny, V., Commowick, O., Pennec, X., Ayache, N.: A log-euclidean framework for statistics on diffeomorphisms. In: MICCAI. pp. 924–931. Springer (2006)
3. Ashburner, J.: A fast diffeomorphic image registration algorithm. *Neuroimage* **38**(1), 95–113 (2007)
4. Ashburner, J., Friston, K.J.: Unified segmentation. *Neuroimage* **26**, 839–851 (2005)
5. Avants, B., Epstein, C., Grossman, M., Gee, J.: Symmetric diffeomorphic image registration with cross-correlation: Evaluating automated labeling of elderly and neurodegenerative brain. *Medical Image Analysis* **12**(1), 26 – 41 (2008)
6. Balakrishnan, G., Zhao, A., Sabuncu, M., Guttag, J., Dalca, A.V.: Voxelmorph: A learning framework for deformable medical image registration. *IEEE Trans. Med. Im.* **38**(8), 1788–00 (2019)
7. Belaroussi, B., Milles, J., Carme, S., Zhu, Y.M., Benoit-Cattin, H.: Intensity non-uniformity correction in mri: existing methods and their validation. *Medical image analysis* **10**(2), 234–246 (2006)
8. Billot, B., Greve, D., Leemput, K.V., Fischl, B., Iglesias, J.E., Dalca, A.V.: A learning strategy for contrast-agnostic mri segmentation (2020)
9. Bookheimer, S.Y., Salat, D.H., Terpstra, M., Ances, B.M., Barch, D.M., Buckner, R.L., Burgess, G.C., et al.: The lifespan human connectome project in aging: An overview. *NeuroImage* **185**, 335 – 348 (2019)
10. Chaitanya, K., Karani, N., Baumgartner, C.F., Becker, A., Donati, O., Konukoglu, E.: Semi-supervised and task-driven data augmentation. In: IPMI. pp. 29–41. Springer (2019)
11. Chollte, F.: Keras: The python deep learning library (2015), <https://keras.io>
12. Dalca, A.V., Balakrishnan, G., Guttag, J., Sabuncu, M.: Unsupervised learning of probabilistic diffeomorphic registration for images and surfaces. *Medical Image Analysis* **57**, 226–236 (2019)
13. Dice, L.R.: Measures of the amount of ecologic association between species. *Ecology* **26**(3), 297–302 (1945)
14. Fischl, B.: Freesurfer. *NeuroImage* **62**(2), 774 – 781 (2012), 20 YEARS OF fMRI
15. Fischl, B., Salat, D.H., Busa, E., Albert, M., Dieterich, M., Haselgrove, C., et al.: Whole brain segmentation: automated labeling of neuroanatomical structures in the human brain. *Neuron* **33**(3), 341–355 (2002)
16. Frackowiak, R., Friston, K., Frith, C., Dolan, R., Price, C., Zeki, S., Ashburner, J., Penny, W.: *Human Brain Function*. Academic Press, 2nd edn. (2003)
17. Guo, C.K.: Multi-modal image registration with unsupervised deep learning. Ph.D. thesis, Massachusetts Institute of Technology (2019)
18. Harms, M.P., Somerville, L.H., Ances, B.M., Andersson, J., Barch, D.M., et al.: Extending the human connectome project across ages: Imaging protocols for the lifespan development and aging projects. *NeuroImage* **183**, 972 – 984 (2018)
19. Hou, Z.: A review on mr image intensity inhomogeneity correction. *International journal of biomedical imaging* **2006** (2006)
20. Iglesias, J.E., Konukoglu, E., Zikic, D., Glocker, B., Van Leemput, K., Fischl, B.: Is synthesizing mri contrast useful for inter-modality analysis? In: MICCAI. pp. 631–638. Springer (2013)
21. Kamnitsas, K., Baumgartner, C., Ledig, C., Newcombe, V., Simpson, J., Kane, A., Menon, D., Nori, A., et al.: Unsupervised domain adaptation in brain lesion segmentation with adversarial networks. In: IPMI. pp. 597–609 (2017)
22. Klein, A., Andersson, J., Ardekani, B.A., Ashburner, J., Avants, B., Chiang, M.C., et al.: Evaluation of 14 nonlinear deformation algorithms applied to human brain MRI registration. *Neuroimage* **46**(3), 786–802 (2009)

23. Krebs, J., Delingette, H., Mailhé, B., Ayache, N., Mansi, T.: Learning a probabilistic model for diffeomorphic registration. *IEEE TMI* **38**(9), 2165–2176 (2019)
24. Krebs, J., Mansi, T., Delingette, H., Zhang, L., Ghesu, F., et al.: Robust non-rigid registration through agent-based action learning. In: *MICCAI*. pp. 344–352 (2017)
25. Milletari, F., Navab, N., Ahmadi, S.A.: V-net: Fully convolutional neural networks for volumetric medical image segmentation. In: *2016 3DV*. pp. 565–571 (2016)
26. Modat, M., Ridgway, G.R., Taylor, Z.A., Lehmann, M., Barnes, J., Hawkes, D.J., et al.: Fast free-form deformation using graphics processing units. *Computer Methods and Programs in Biomedicine* **98**(3), 278 – 284 (2010), hP-MICCAI 2008
27. Mugler III, J.P., Brookeman, J.R.: Three-dimensional magnetization-prepared rapid gradient-echo imaging (3d mp rage). *MRM* **15**(1), 152–157 (1990)
28. Perlin, K.: An image synthesizer. *ACM Siggraph Computer Graphics* **19**(3), 287–296 (1985)
29. Puonti, O., Iglesias, J.E., Leemput, K.V.: Fast and sequence-adaptive whole-brain segmentation using parametric bayesian modeling. *NeuroIm.* **143**, 235–249 (2016)
30. Pustina, D., Cook, P.: Anatomy of an antsregistration call (2017), <https://github.com/ANTsX/ANTs/wiki/Anatomy-of-an-antsRegistration-call>
31. Qin, C., Shi, B., Liao, R., Mansi, T., Rueckert, D., Kamen, A.: Unsupervised deformable registration for multi-modal images via disentangled representations. In: *IPMI*. pp. 249–261. Springer (2019)
32. Reuter, M., Rosas, H.D., Fischl, B.: Highly accurate inverse consistent registration: A robust approach. *NeuroImage* **53**(4), 1181 – 1196 (2010)
33. Roche, A., Malandain, G., Pennec, X., Ayache, N.: The correlation ratio as a new similarity measure for multimodal image registration. *MICCAI* pp. 1115–24 (1998)
34. Rohé, M., Datar, M., Heimann, T., Sermesant, M., Pennec, X.: SVF-Net: Learning deformable image registration using shape matching. *MICCAI* pp. 266–274 (2017)
35. Rohr, K., Stiehl, H.S., Sprengel, R., Buzug, T.M., Weese, J., Kuhn, M.: Landmark-based elastic registration using approximating thin-plate splines. *IEEE TMI* **20**(6), 526–534 (2001)
36. Ronneberger, O., Fischer, P., Brox, T.: U-net: Convolutional networks for biomedical image segmentation. *CoRR* **abs/1505.04597** (2015)
37. Rueckert, D., Sonoda, L.I., Hayes, C., Hill, D.L., Leach, M.O., Hawkes, D.J.: Nonrigid registration using free-form deformations: application to breast mr images. *IEEE TMI* **18**(8), 712–721 (1999)
38. Sokooti, H., de Vos, B., Berendsen, F., Lelieveldt, B.P., Išgum, I., Staring, M.: Nonrigid image registration using multi-scale 3d convolutional neural networks. In: *MICCAI*. pp. 232–239. Springer (2017)
39. Van Leemput, K., Maes, F., Vandermeulen, D., Suetens, P.: Automated model-based tissue classification of mr images of the brain. *IEEE TMI* **18**, 897–908 (1999)
40. Vercauteren, T., Pennec, X., Perchant, A., Ayache, N.: Diffeomorphic demons: Efficient non-parametric image registration. *NeuroImage* **45**(1), S61–S72 (2009)
41. Viola, P., Wells III, W.M.: Alignment by maximization of mutual information. *International journal of computer vision* **24**(2), 137–154 (1997)
42. de Vos, B.D., Berendsen, F.F., Viergever, M.A., Sokooti, H., Staring, M., Išgum, I.: A deep learning framework for unsupervised affine and deformable image registration. *Medical image analysis* **52**, 128–143 (2019)
43. Weiner, M.W.: Alzheimers disease neuroimaging initiative (ADNI) database (2003), <http://adni.loni.usc.edu>
44. Xu, J., Zhang, M., Turk, E.A., Zhang, L., Grant, P.E., Ying, K., Golland, P., Adalsteinsson, E.: Fetal pose estimation in volumetric mri using a 3d convolution neural network. In: *MICCAI*. pp. 403–410. Springer (2019)
45. Zhao, A., Balakrishnan, G., Durand, F., Guttag, J.V., Dalca, A.V.: Data augmentation using learned transforms for one-shot medical image segmentation. *CoRR* **abs/1902.09383** (2019)